
Estimating Barycenters of Measures in High Dimensions

Samuel Cohen

Department of Computer Science
University College London

Michael Arbel

Gatsby Computational Neuroscience Unit
University College London

Marc Peter Deisenroth

Department of Computer Science
University College London

Abstract

Barycentric averaging is a principled way of summarizing populations of measures. Existing algorithms for estimating barycenters typically parametrize them as weighted sums of Diracs and optimize their weights and/or locations. However, these approaches do not scale to high-dimensional settings due to the curse of dimensionality. In this paper, we propose a scalable and general algorithm for estimating barycenters of measures in high dimensions. The key idea is to turn the optimization over measures into an optimization over generative models, introducing inductive biases that allow the method to scale while still accurately estimating barycenters. We prove local convergence under mild assumptions on the discrepancy showing that the approach is well-posed. We demonstrate that our method is fast, achieves good performance on low-dimensional problems, and scales to high-dimensional settings. In particular, our approach is the first to be used to estimate barycenters in thousands of dimensions.

1 Introduction

Barycenters are principled summaries (averages) of probability measures [1]. They are defined with respect to a similarity metric on the space of measures. Computing barycenters has been extensively studied by Agueh and Carlier [1], Benamou et al. [6], Cuturi and Doucet [15], and Luise et al. [30], and barycenters have been used in computer vision [23], economics [11], Bayesian inference [38], physics [35], and machine learning [17, 20]. For instance, Dognin et al. [17] used Wasserstein barycenters to find a consensus between models trained in the context of multi-class classification. Computing barycenters of probability measures is challenging, due to the need to optimize over spaces of measures. Current approaches typically use compactly-supported basis functions, in particular Diracs, to parametrize barycenters and optimize their weights and/or locations [15, 30]. The strictly local property of these functions requires an exponentially increasing number of basis functions as the dimensionality of their domain increases. As a result of this ‘curse of dimensionality’, these methods are typically restricted to low-dimensional problems ($\mathbb{R}^{\leq 3}$).

In this paper, we introduce an algorithm for estimating barycenters of measures that applies to high-dimensional settings. The main idea is to turn the optimization over measures into a more tractable optimization over a space of generative models. Specifically, we parametrize the barycenter with a latent measure and a parametric model that maps samples from the latent space to the target space. We thus leverage a parametric generator, consisting of global basis functions, which is in contrast to parametrizing the weights and locations directly. This allows us to apply our algorithm to barycentric problems at an unprecedented scale in terms of dimensions and support (e.g., in image

space $\mathbb{R}^{\text{width} \times \text{height} \times \text{channels}}$). We demonstrate that our approach leverages the problem structure to obtain computational speedups by incorporating inductive biases. We also prove local convergence of our proposed algorithm to stationary points for common discrepancies.

The averaging properties of barycenters heavily rely on the geometry induced by the considered discrepancy. However, previous approaches were tailored to particular distances, and mainly focused on algorithms for computing Wasserstein and Gromov-Wasserstein barycenters. By contrast, our algorithm is also general in the sense that it can be used with different discrepancies, including maximum mean discrepancy (MMD) [24], entropic-regularized Wasserstein [14] and Gromov-Wasserstein [35]. It enables us to analyze the different barycentric properties through the same lens.

2 Barycenters of Probability Measures

We consider the problem of computing barycenters of probability measures defined on a subset \mathcal{X} of \mathbb{R}^d . We denote by $\mathcal{M}_1^+(\mathcal{X})$ the set of such measures on \mathcal{X} and define the probability simplex $\Delta_P := \{\boldsymbol{\beta} \in \mathbb{R}^P : \sum_{p=1}^P \beta_p = 1, \beta_p \geq 0 \ \forall p\}$. The barycenter of P probability measures $\mu_1, \dots, \mu_P \in \mathcal{M}_1^+(\mathcal{X})$ weighted by a vector $\boldsymbol{\beta} \in \Delta_P$ can be expressed as the optimal measure μ^* solving the optimization problem [1]

$$\mu^* = \arg \min_{\mu \in \mathcal{M}_1^+(\mathcal{X})} \sum_{p=1}^P \beta_p D(\mu, \mu_p), \quad (1)$$

where $D : \mathcal{M}_1^+(\mathcal{X}) \times \mathcal{M}_1^+(\mathcal{X}) \rightarrow \mathbb{R}^+$ is a discrepancy between measures. Depending on the choice of D , barycenters have significantly different properties. We now discuss two families of barycenters obtained when using the Wasserstein distance and the MMD as discrepancy D , while providing novel results about their properties extending the work by Agueh and Carlier [1], Anderes et al. [2], and Bottou et al. [9].

2.1 Wasserstein Barycenters

The k -Wasserstein distance between two measures $\mu_x, \mu_y \in \mathcal{M}_1^+(\mathcal{X})$ is defined as [41]

$$\mathcal{W}_k(\mu_x, \mu_y) = \min_{\pi \in U(\mu_x, \mu_y)} \left(\int_{\mathcal{X} \times \mathcal{X}} d^k(\mathbf{x}, \mathbf{y}) d\pi(\mathbf{x}, \mathbf{y}) \right)^{\frac{1}{k}}, \quad (2)$$

where $d : \mathcal{X} \times \mathcal{X} \rightarrow \mathbb{R}$ is a distance representing the cost of transporting a unit of mass from $\mathbf{x} \in \mathcal{X}$ to $\mathbf{y} \in \mathcal{X}$, and $U(\mu_x, \mu_y)$ is the set of joint distributions with marginals μ_x, μ_y . Intuitively, \mathcal{W}_k in (2) corresponds to the minimal expected cost of transporting mass from μ_x to μ_y according to an optimal plan $\pi \in U(\mu_x, \mu_y)$. Importantly, it does not require μ_x and μ_y to share the same support.

Characterization of Wasserstein Barycenters Agueh and Carlier [1] showed that, under the assumption that at least one of the probability measures is absolutely continuous, the barycenter problem (in the case $k = 2$, and $d = L^2$) is equivalent to a generalization of the optimal transport problem defined in (2), called the *multi-marginal optimal transport problem*:

$$\min_{\pi \in U(\mu_1, \dots, \mu_P)} \int \sum_{p=1}^P \beta_p \|\mathbf{x}_p - T(\mathbf{X})\|^2 d\pi(\mathbf{x}_1, \dots, \mathbf{x}_P). \quad (3)$$

Here, $U(\mu_1, \dots, \mu_P)$ is the set of joint distributions with marginals μ_1, \dots, μ_P , \mathbf{X} is the concatenated vector $\mathbf{X} := (\mathbf{x}_1, \dots, \mathbf{x}_P)$, and $T(\mathbf{X}) := \sum_{p=1}^P \beta_p \mathbf{x}_p$. The barycenter is then described by means of the McCann's interpolant [31] if at least one μ_i admits a density. This means that a sample \mathbf{Y} from the barycenter distribution can be obtained by computing the Euclidean barycenter of samples $\mathbf{X} = (\mathbf{x}_1, \dots, \mathbf{x}_P)$ from an optimal coupling π of (3), i.e., $\mathbf{Y} = T(\mathbf{X})$. Anderes et al. [2] obtained a similar characterization for discrete measures. Unfortunately, those results cannot be directly applied to the case where all measures are supported on potentially disjoint low-dimensional manifolds which are neither discrete nor do they admit a density. In Theorem 1, we provide a generalization of those results for arbitrary probability measures (beyond discrete or absolutely continuous probability measures) and provide a proof in Appendix B.

Theorem 1. (*2-Wasserstein Barycenter*): When the discrepancy between measures is $D = \mathcal{W}_2^2$, and d is the Euclidean L^2 norm, the barycenter μ^* of measures $\mu_1, \dots, \mu_P \in \mathcal{M}_1^+(\mathcal{X})$ with weights $\beta \in \Delta_P$ is expressed in terms of the optimal solution π of (3) as:

$$\mathbf{Y} \sim \mu^* \iff \mathbf{Y} = T(\mathbf{X}), \quad \mathbf{X} \sim \pi, \quad (4)$$

As an illustration of Theorem 1, Figure 1(a) shows that the 2-Wasserstein barycenter of four isotropic Gaussians located on the corners of a square with width $s = 10$ indeed displaces the mass proportionally to the weights (toward the mode with the highest weight). Results in Agueh and Carlier [1] and Anderes et al. [2], and their extension in this paper to arbitrary probability measures enable us to interpret the shape of the 2-Wasserstein barycenter, in particular its interpolation properties. This enables directly extending the interpretation of the displacement geodesics of Bottou et al. [9]

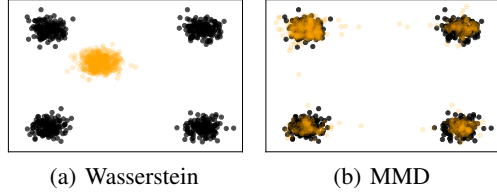


Figure 1: Barycenter (orange) of four Gaussians (black) with respect to (a) \mathcal{W}_ϵ ; (b) MMD. Top-left Gaussian has three times the weight of the others.

($P = 2$) to the case $P \geq 2$. Also, the optimal coupling of Agueh and Carlier [1] is deterministic (because one of the measure is absolutely continuous), whilst in the most general case the coupling is stochastic, which our theorem allows. The proposed generalization is thus analogous to the relaxation of the classical Monge formulation [32] (deterministic) of the Wasserstein distance to the Kantorovich formulation [27] (stochastic).

Computing Wasserstein Barycenters Most previous approaches to computing barycenters of measures can be categorized into fixed [15, 18, 39] and free [13, 15, 30] support. Fixed-support approaches choose a finite set of locations $x_1, \dots, x_N \in \mathcal{X}$, parametrize the barycenter as a weighted sum of Diracs $\mu = \sum_{n=1}^N a_n \delta_{x_n}$, and optimize (1) with respect to the weights a_n . Free-support approaches typically optimize both locations x_n and weights a_n by alternated optimization.

In general, computing the Wasserstein barycenter requires evaluating the Wasserstein distance in (2) several times, which is computationally challenging. Recent advances provide algorithms to solve (2) approximately with a lower computational cost. Cuturi [14] proposed to solve a regularized version of (2) by adding a small (relative) *entropic* term for regularization purposes. This leads to a smooth convex objective

$$\mathcal{W}_{k,\epsilon}^k(\mu_x, \mu_y) = \min_{\pi \in U(\mu_x, \mu_y)} \int_{\mathcal{X} \times \mathcal{X}} d^k(\mathbf{x}, \mathbf{y}) d\pi(\mathbf{x}, \mathbf{y}) + \epsilon \text{KL}(\pi || \mu_x \otimes \mu_y), \quad (5)$$

for which optimization scales considerably better. Here, $\epsilon \geq 0$ controls the regularization. For simplicity, we refer to \mathcal{W}_ϵ as the entropic-regularized Wasserstein with general cost. (5) can be solved by the Sinkhorn–Knopp algorithm [37], which has computational complexity $\mathcal{O}(\frac{N^2}{\epsilon^2})$ and can be parallelized on GPUs. Benamou et al. [6] and Cuturi and Doucet [15] proposed respectively fixed- and free-support barycentric approaches that leverage (5) to speed up barycenter computation.

The objective in (5) is biased since in general $\mathcal{W}_\epsilon(\mu, \mu) \neq 0$ [22]. Thus, (5) does not define a distance. Moreover, the bias can lead to possibly wrong minima during optimization [5]. To alleviate this issue, Genevay et al. [21] introduced the Sinkhorn divergence

$$\mathcal{S}\mathcal{W}_\epsilon = 2\mathcal{W}_\epsilon(\mu_x, \mu_y) - \mathcal{W}_\epsilon(\mu_x, \mu_x) - \mathcal{W}_\epsilon(\mu_y, \mu_y), \quad (6)$$

which removes that bias. Equation (6) is symmetric, non-negative, and unbiased while still approximating the Wasserstein distance for $\epsilon \rightarrow 0$. Hence, the Wasserstein barycenter can be in principle estimated using the Sinkhorn divergence instead of the less tractable Wasserstein distance [30].

However, these approaches hardly scale to high-dimensional problems due to the need to optimize the locations x_n . The number of parameters we need to optimize thus scales exponentially with the dimensionality of the space, which makes them inapplicable to high-dimensional problems, such as considering datasets of images (where individual x_n are images). Indeed, previous approaches tackle problems in $\mathbb{R}^{\leq 3}$ [6, 8, 13, 15, 18, 30].

2.2 Maximum Mean Discrepancy Barycenters

The maximum mean discrepancy [24] is a distance between probability distributions that relies on a positive definite kernel $k : \mathcal{X} \times \mathcal{X} \rightarrow \mathbb{R}$ as a measure of similarity between pairwise samples:

$$\text{MMD}(\mu_x, \mu_y)^2 := \mathbb{E}_{\mathbf{x}, \mathbf{x}' \sim \mu_x} [k(\mathbf{x}, \mathbf{x}')] + \mathbb{E}_{\mathbf{y}, \mathbf{y}' \sim \mu_y} [k(\mathbf{y}, \mathbf{y}')] - 2\mathbb{E}_{\mathbf{x} \sim \mu_x, \mathbf{y} \sim \mu_y} [k(\mathbf{x}, \mathbf{y})]. \quad (7)$$

Here the first two terms compute the average similarity within each of μ_x and μ_y while the last term computes the average similarity between samples from μ_x and μ_y . Unlike the Wasserstein distance, estimating the MMD using samples from μ_x and μ_y is straightforward [24]. Equation (7) has another formulation based on the notion of *kernel mean embeddings*, from which the MMD barycenter can be easily characterized. The *kernel mean embedding* [33] is a map η from probability space to the reproducing kernel Hilbert space (RKHS) \mathcal{H} corresponding to the kernel k :

$$\eta : \mathcal{M}_1^+(\mathcal{X}) \rightarrow \mathcal{H}, \quad \eta(\mu_x) = \mathbb{E}_{\mathbf{x} \sim \mu_x} [k(\cdot, \mathbf{x})]. \quad (8)$$

Hence, each probability measure is represented by a function in the RKHS, thereby leveraging the representational power of the embedding η . This allows us to measure similarity between distributions in terms of an inner product between their mean embeddings, so that

$$\text{MMD}(\mu_x, \mu_y) := \|\eta(\mu_x) - \eta(\mu_y)\|_{\mathcal{H}}. \quad (9)$$

where the norm $\|\cdot\|_{\mathcal{H}}$ is derived from the RKHS inner product defined on \mathcal{H} .

Characterizing the MMD Barycenter Using the notion of mean embeddings, it is easy to characterize the MMD barycenter. Equation (9) suggests to first represent each measure μ_p in (1) by its mean embedding $\eta(\mu_p)$ then find the barycenter η^* of those embeddings in the RKHS \mathcal{H} . It turns out that η^* is simply a weighted sum of $(\eta(\mu_p))_{1 \leq p \leq P}$ with weights β . Finally, we recover the probability distribution represented by η^* , which is exactly the MMD barycenter and has an explicit expression. Theorem 2 provides such an expression with a proof in Appendix C.

Theorem 2. (MMD Barycenter): *If $D = \text{MMD}^2$, the barycenter of measures $\mu_1, \dots, \mu_P \in \mathcal{M}_1^+(\mathcal{X})$ with weights $\beta \in \Delta_P$ is the mixture of measures*

$$\mu^* := \sum_{p=1}^P \beta_p \mu_p \in \mathcal{M}_1^+(\mathcal{X}). \quad (10)$$

Theorem 2 can be seen as a direct extension of results describing the geodesic structure induced by the MMD (Th. 5.3 in Bottou et al. [9]). It also suggests a basic generative process for sampling from MMD barycenters: (i) generate a draw $z \sim \text{Categorical}_P(\beta)$; (ii) sample from the chosen measure μ_z . Hence, the MMD barycenter allocates mass only at locations where its component measures allocate mass, proportionally to the barycentric weights, which is in stark contrast to the properties of the 2-Wasserstein barycenter. For instance, Figure 1(b) shows that the MMD barycenter consists of a mixture of the measures, with three times the weight on the top-left location. As expected, there is mass on all measures proportionally to the barycentric weights β .

3 Estimating Barycenters Using Generative Models

In the following, we propose an algorithm for estimating barycenters (1) between P probability measures with discrepancies including MMD with optimized kernel [3], \mathcal{W}_ϵ [14] and \mathcal{SW}_ϵ [22]. The key idea behind our algorithm is to approximate the optimization over the intractable space of measures by a parametric optimization over a space of generative models. This allows us to incorporate structural inductive biases, enabling our algorithm to scale in high dimensions. We also prove local convergence for popular choices of discrepancies.

3.1 Algorithm

We approximate the barycenter by a parametric generative model \mathbb{P}_θ which is a probability measure in $\mathcal{M}_1^+(\mathcal{X})$ parameterized by a finite dimensional vector θ .

Those models are typically defined as push-forwards of a latent measure $\rho \in \mathcal{M}_1^+(\mathcal{Z})$ on a lower-dimensional space through a generator function $G_\theta : \mathcal{Z} \rightarrow \mathcal{X}$. This means that a sample \mathbf{x} from

\mathbb{P}_θ is obtained by first sampling z from the latent ρ , then mapping it through G_θ , i.e.: $x = G_\theta(z)$. More concisely, we simply write $\mathbb{P}_\theta = G_{\theta\#\rho}$.

We then propose to approximate the barycenter by solving a parametric version of the barycentric problem (1):

$$\theta^* = \arg \min_{\theta} L(\theta), \quad L(\theta) := \sum_{p=1}^P \beta_p l_p(\theta), \quad l_p(\theta) := D(G_{\theta\#\rho}, \mu_p), \quad (11)$$

where D is a discrepancy between measures. The optimization problem in (11) can be solved by stochastic gradient descent as described in Algorithm 1 (Appendix D). At each training iteration, the algorithm receives a batch of data points from the individual measures as well as a batch of samples from the generator. Those are then used to compute stochastic gradients $g_p(\theta_t)$ of the distances between the generator and each of the measures μ_p . The parameter θ_t is then updated by running gradient descent steps using the stochastic barycentric gradient $\sum_{p=1}^P \beta_p g_p(\theta_t)$. We note that the discrepancy D needs to be well-defined for measures with discrete support as the barycenter is only accessible through its samples. This is a fundamentally different approach from prior works that approximate the barycenter as a Dirac mixture.

Inductive Biases We can incorporate prior knowledge on the form of the barycenter through the generator’s structure (e.g., CNNs for barycenters of images) and leverage global basis functions (neural networks in particular). This enables scaling to high-dimensional settings, unlike Dirac-based approaches which optimize locations of particles in a high dimensional space and thus suffer from the curse of dimensionality. Note that G_θ is not restricted to being a neural network, and domain knowledge can enable more efficient learning. For instance, if we know that the actual barycenter is a Gaussian, we can set $\rho = \mathcal{N}(\mathbf{0}, \mathbf{I})$, $G_\theta(z_n) = \mathbf{S}^{\frac{1}{2}} z_n + \mathbf{m}$ and optimize the mean \mathbf{m} and covariance \mathbf{S} using our algorithm as shown empirically in Section 4.

Optimization Using $D = \text{MMD}(\mathbb{P}_\theta, \mathbb{P})$ with a fixed kernel k is ineffective when training on datasets of natural images, as the training signal may be small where $\mathbb{P}_\theta \neq \mathbb{P}$ [28]. To alleviate this issue, deep kernels $k_{f_\psi}(x, y) = k(f_\psi(x), f_\psi(y))$ are trained in an adversarial fashion to learn the function f_ψ as well as the generator, similarly to Arbel et al. [3], Binkowski et al. [7], and Li et al. [28], allowing the gradient signal to increase at locations where $\mathbb{P}_\theta \neq \mathbb{P}$. Then, D is of the form

$$\text{SMMD}^2(\mathbb{P}_\theta, \mathbb{P}) := \sup_{f_\psi \in \mathcal{E}} \text{MMD}_\psi^2(G_{\theta\#\rho}, \mathbb{P}), \quad (12)$$

where we assume that all $f_\psi \in \mathcal{E}$ are continuously parametrized by $\psi \in \Psi$ with Ψ compact. Similar issues arise when using \mathcal{W}_ϵ and $S\mathcal{W}_\epsilon$. Therefore, analogous adversarial formulations of these discrepancies were advocated [10, 22]. All these approaches require a careful regularization of the critic, which can be done by penalizing its gradient [3, 7, 25] or weight clipping [4].

Special Cases Firstly, the special case $P = 1$ corresponds to the traditional implicit generative model objective. In that setting, different kinds of discrepancies D have been considered, including MMD [19, 28], 1-Wasserstein [4, 25], Sinkhorn divergence [22], and \mathcal{GW}_ϵ [10]. Also, from a purely computational perspective, Su et al. [40] train a Wasserstein GAN on a single dataset by randomly splitting that dataset into P subsets and minimizing the average 1-Wasserstein between samples from the GAN and from those subsets. This is a special case of our framework in which the individual measures are all equal to the same data distribution. This implies that the barycenter coincides with such data distribution leading to a significantly simpler problem. In the case where all measures are Gaussians, Chewi et al. [12] derive explicitly the gradients of the Wasserstein barycenter functional with respect to the mean and variance of the barycenter and use SGD to learn it.

Remark 1. *In the MMD case, the barycenter computed using our algorithm targets the mixture of the datasets. In multimodal problems, it enables training with larger batches per modes as training scales as $O(PN^2)$ where N is the number of samples per mode and P the number of modes, instead of $O(P^2N^2)$ for GANs.*

3.2 Convergence Analysis

The non-convexity of the loss (11) with respect to the model parameters θ makes it hard to guarantee global convergence. However, we study local convergence to stationary points which is challenging on its own since the divergence D often results from an optimization procedure. Only recently, Sanjabi et al. [36] provided related results for the regularized Wasserstein distance. We extend those results to the case of the barycenter problem and to SMMD which relies on a different technique.

3.2.1 Smoothness

Typical local convergence results rely on notions of smoothness. *Lipschitz smoothness* is the most commonly used notion to guarantee local convergence.

Definition 3. A function $L : \Theta \mapsto \mathbb{R}$ is M -Lipschitz smooth if there exists an $M \geq 0$, such that

$$\|\nabla L(\theta) - \nabla L(\theta')\| \leq M\|\theta - \theta'\| \quad \forall \theta, \theta' \in \Theta. \quad (13)$$

Lipschitz smoothness of a function L requires that the gradient of L exists and is Lipschitz continuous. Sanjabi et al. [36] showed that entropic-regularized Wasserstein GANs ((11) with $P = 1$ and $D = \mathcal{W}_\epsilon$) are M -Lipschitz smooth with respect to the generator parameters θ .

In Proposition 4, we extend this result to barycenters ($P \geq 1$) when $D = \mathcal{SW}_\epsilon$ as in (6).

Proposition 4. Assume \mathcal{X} and \mathcal{Z} are compact and G_θ is Lipschitz and Lipschitz-smooth. Then, the barycenter objective

$$L(\theta) := \sum_{p=1}^P \beta_p \mathcal{SW}_\epsilon(G_{\theta\#\rho}, \mu_p) \quad (14)$$

is M -Lipschitz smooth. Proof: See Appendix A.

In the case of the optimized MMD, the discriminator is also learned leading to a non-concave problem. Therefore, the approach of Sanjabi et al. [36] cannot be directly applied to guarantee M -Lipschitz smoothness of the resulting objective with respect to generator parameters θ . Instead, we show that MMD satisfies a weaker notion of regularity called *weak convexity*, which turns out to be sufficient to guarantee local convergence [16]:

Definition 5. A function $L : \Theta \rightarrow \mathbb{R}$ is C -weakly convex if there exists a positive constant C , such that $L(\theta) + C\|\theta\|^2$ is convex.

Proposition 6. Assume the kernel k is Lipschitz and Lipschitz-smooth and functions $f_\psi \in \mathcal{E}$ are Lipschitz, Lipschitz-smooth, and absolutely continuous with respect to the parameters ψ and inputs \mathbf{x} . Further assume G_θ is Lipschitz and Lipschitz-smooth in θ . Then,

$$L(\theta) := \sum_{p=1}^P \beta_p \text{SMMD}^2(G_{\theta\#\rho}, \mu_p) \quad (15)$$

is weakly convex and Lipschitz. Proof: See Appendix A.

Proposition 6 states that the optimized MMD is *weakly convex* and Lipschitz provided that the discriminator satisfies additional smoothness constraints.

3.2.2 Local Convergence

We now show that whenever Proposition 4 or Proposition 6 hold, stochastic gradient descent (SGD) converges to a local optimum. While Proposition 4 and Proposition 6 are sufficient to guarantee convergence to a stationary value θ^* for gradient descent or SGD, it requires access to an unbiased estimate of the gradient of L . In practice, this is not possible as L is estimated by approximately solving an optimization problem. Instead, we propose to use a similar setting as in Sanjabi et al. [36], where we assume access to an unbiased estimate of a direction g that approximates $\nabla L(\theta)$ to a precision δ . In other words, g satisfies: $\|\nabla L(\theta) - g\|^2 \leq \delta^2$, and \tilde{g} is an unbiased stochastic estimator of g , i.e.: $\mathbb{E}[\tilde{g}] = g$ which we assume we have access to. Such an estimate can be obtained by performing a few steps of gradient descent on the discriminator, in the case of the optimized MMD, and then evaluating the gradient of the resulting loss with respect to θ on new samples. We further assume that the noise in \tilde{g} has a bounded variance, i.e., $\mathbb{E}[\|g - \tilde{g}\|^2] \leq \sigma^2$, and we define $\Delta := L(\theta_0) - \inf_\theta L(\theta)$ as the initial regret.

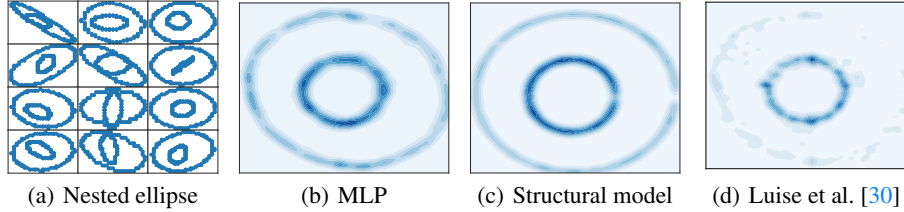


Figure 2: Sinkhorn barycenter of 30 nested ellipses, of which a subset is displayed in (a) using (b) the MLP parametrization, (c) the nested ellipses parametrization, (d) Luise et al. [30].

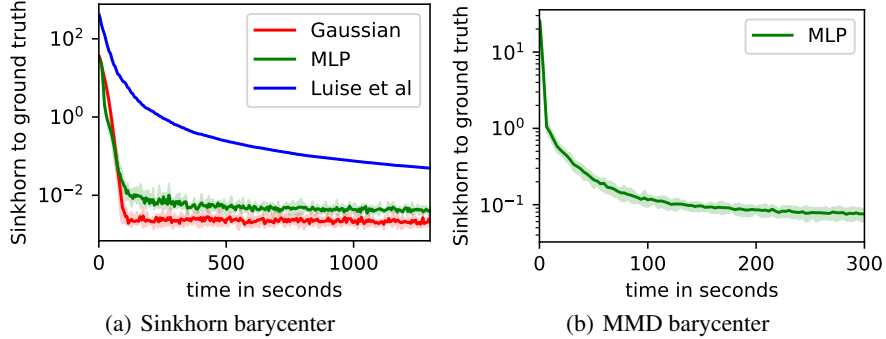


Figure 3: Convergence plot of the computation of the barycenter of 15 Gaussians w.r.t. (a) \mathcal{SW}_ϵ using MLP/Gaussian parametrization, and Luise et al. [30], (b) w.r.t. MMD via MLP parametrization.

Theorem 7 ([36]). *Assume $\|\nabla L(\theta) - g\|^2 \leq \delta^2$, $\mathbb{E}[\|g - \tilde{g}\|^2] \leq \sigma^2$ and $\mathbb{E}[\tilde{g}] = g$. Also, if $L(\theta)$ is M -Lipschitz smooth (as in Proposition 4), then setting the learning rate to $\alpha := \sqrt{\frac{2\Delta}{M\sigma^2}}$ yields*

$$\min_{0 \leq t \leq T-1} \mathbb{E}[\|\nabla L(\theta_t)\|^2] \leq \sqrt{\frac{8\Delta M\sigma^2}{T}} + \delta^2. \quad (16)$$

Theorem 7 shows that stochastic gradient methods converge to a stationary point when Proposition 4 holds. If $L(\theta)$ is only C -weakly convex as in Proposition 6, local convergence still holds [16].

4 Experiments

We now demonstrate that leveraging parametric functions and encoding inductive biases can scale the computation of barycenters to high dimensions, while still recovering accurate barycenters. We provide extensive experimental details in the Appendix.

4.1 Traditional Barycentric Problems

We start with classical barycenter problems to demonstrate our approach yields sensible solutions to the barycentric problem (1), and that leveraging structure can speed up computations.

Nested ellipses We consider the computation of the \mathcal{SW}_ϵ barycenter of $P = 30$ nested ellipses, reproducing the example of Cuturi and Doucet [15] and Luise et al. [29, 30]. We compare to the algorithm proposed by Luise et al. [30]. We consider two approaches to parametrizing the generator G_θ , (i) using a multi-layer perceptron (MLP) as G_θ and (ii) exploiting inductive biases by parametrizing two ellipses (θ : axis lengths and centers of both ellipses). Figure 2 shows that both approaches recover the barycenter, and obtain a similar but more accurate solution than the approach proposed in [30] (under a time budget). In particular, there is significantly more support on the ground truth barycenter due to the global nature of our algorithm.



Figure 4: Samples from our MMD Barycenter of CelebA males and females.

Gaussians We consider a setting in which structural knowledge can be leveraged, namely computing MMD and SW_ϵ barycenters of $P = 15$ isotropic Gaussians. We consider (i) using an MLP as G_θ (both MMD and SW_ϵ) and (ii) parametrizing the mean and variance of a Gaussian for Sinkhorn. This exploits the fact that the barycenter of Gaussians w.r.t. Wasserstein is a Gaussian, so that the closed-form barycenter belongs to the parametrized family of models we consider (approximately as Sinkhorn approximates Wasserstein). Figure 3(a) illustrates that (i) our algorithm converges to a stationary point (see Section 3.2.2) and that the gradient bias is negligible; (ii) structural knowledge can lead to faster and more accurate approximations as the Gaussian parametrization converges to a better solution than the MLP one; (iii) our algorithm is significantly faster than Luise et al. [30] (we provide a further discussion of runtimes and implementations in the Appendix). Also, Figure 3(b) shows local convergence to a good stationary point (close to the known ground truth barycenter) of the model when computing the MMD barycenter.

4.2 Barycenters of natural images

We now demonstrate that the combination of structural knowledge and parametric models can scale barycentric computations to high-dimensions. Previous papers considered problems in which measures are supported on $\mathbb{R}^{\leq 3}$. Even in experiments with images, these were considered as densities on a 2D space [15, 30]. In the following, we consider a significantly more challenging setting in which each measure consists of a dataset of 10^4 – 10^5 images of dimensionality 10^3 – 10^5 . We only consider the MMD barycenter as in this setting, a mixture behavior is desired.

MNIST We compute the barycenter of 10 measures μ_0, \dots, μ_9 , where μ_m corresponds to the dataset of the m^{th} MNIST digit. Each measure consists of approximately 5,000 samples in a 32×32 -dimensional space. Figure 5 shows that the MMD barycenter generates meaningful samples from all classes, as expected from the mixture behavior of MMD barycenters (see Section 2.2).

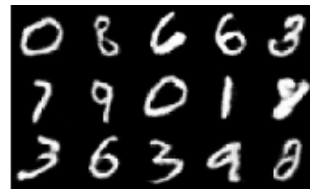


Figure 5: Samples of digits from our MMD barycenter.

CelebA We now compute the barycenter of two measures, CelebA males and females, each having approximately 100,000 locations (images). Images are re-scaled to $3 \times 128 \times 128$ pixels, so that each (males/females) lives in an approximately 50,000-dimensional space. We use deep convolutional generators and critics to leverage the structural knowledge about the input locations (images). Figure 4 illustrates that the MMD barycenter generates meaningful high-quality samples from both measures, in a setting where all other approaches to barycenter computations are not applicable. Overall, (i) expected barycentric geometric properties are observed in high-dimensional problems; (ii) using structural knowledge (here a CNN) enables approximating barycentric problems at unprecedented scale dimensionally.

5 Conclusion

We proposed an algorithm for estimating high-dimensional barycenters of probability measures with respect to general choices of discrepancies. The key idea is to formulate the optimization over the space of probability measures as an optimization over parametric generative models, which alleviates the curse of dimensionality, and enables incorporating explicit inductive biases. Furthermore, we proved local convergence of our algorithm to stationary points under mild assumptions on the discrepancy considered. We applied our algorithm to problems at an unprecedented scale, which includes estimating barycenters of measures with more than 10^5 locations in over 10^4 dimensions, while previous approaches were typically constrained to problems in $\mathbb{R}^{\leq 3}$.

Broader Impact

The algorithm developed in this paper can enable the scalable use of barycenters as principled summaries of large and high-dimensional measures. These summaries leverage the geometry of the ground space, which can lead to a better notion of averaging. There are areas in which providing sensible summaries of potentially large-scale data is essential, for instance in medical imaging. Barycenters have indeed been used in this setting, in particular for summarizing [23], or training multi-task regression models [26] on neuro-imaging data. This could potentially help doctors to make better informed diagnosis in a shorter amount of time. We expect that our algorithm can lead to a wider applicability of barycenters as means of summarizing high-dimensional datasets.

Acknowledgements

We are grateful to Giulia Luise for providing us code and data for experiments, and for providing feedback on the draft. SC was supported by the Engineering and Physical Sciences Research Council (grant number EP/S021566/1).

References

- [1] M. Agueh and G. Carlier. Barycenters in the Wasserstein Space. *SIAM Journal on Mathematical Analysis*, 43(2):904–924, 2011. Cited on pages 1–3.
- [2] E. Anderes, S. Borgwardt, and J. Miller. Discrete Wasserstein Barycenters: Optimal Transport for Discrete Data. *Mathematical Methods of Operations Research*, 84, 2015. Cited on pages 2, 3.
- [3] M. Arbel, D. Sutherland, M. Bikowski, and A. Gretton. On Gradient Regularizers for MMD GANs. In *NeurIPS*, 2018. Cited on pages 4, 5.
- [4] M. Arjovsky, S. Chintala, and L. Bottou. Wasserstein Generative Adversarial Networks. In *ICML*, 2017. Cited on page 5.
- [5] M. G. Bellemare, I. Danihelka, W. Dabney, S. Mohamed, B. Lakshminarayanan, S. Hoyer, and R. Munos. The Cramer Distance as a Solution to Biased Wasserstein Gradients. *arXiv:1705.10743*, 2018. Cited on page 3.
- [6] J.-D. Benamou, G. Carlier, M. Cuturi, L. Nenna, and G. Peyré. Iterative Bregman Projections for Regularized Transportation Problems. *SIAM Journal on Scientific Computing*, 2(37):A1111–A1138. Cited on pages 1, 3.
- [7] M. Binkowski, D. J. Sutherland, M. Arbel, and A. Gretton. Demystifying MMD GANs. In *ICLR*, 2018. Cited on pages 5, 16.
- [8] N. Bonneel, J. Rabin, G. Peyré, and H. Pfister. Sliced and Radon Wasserstein Barycenters of Measures. *Journal of Mathematical Imaging and Vision*, 1(51):22–45, 2015. Cited on page 3.
- [9] L. Bottou, M. Arjovsky, D. Lopez-Paz, and M. Oquab. Geometrical Insights for Implicit Generative Modeling. In *Lecture Notes in Computer Science*. Springer, 2017. Cited on pages 2–4.
- [10] C. Bunne, D. Alvarez-Melis, A. Krause, and S. Jegelka. Learning Generative Models Across Incomparable Spaces. In *ICML*, 2019. Cited on page 5.
- [11] G. Carlier, A. Oberman, and E. Oudet. Numerical Methods for Matching for Teams and Wasserstein Barycenters. *ESAIM*, 2015. Cited on page 1.

- [12] S. Chewi, T. Maunu, P. Rigollet, and A. J. Stromme. Gradient Descent Algorithms for Bures-Wasserstein Barycenters. *arXiv:2001.01700*, 2020. Cited on page 5.
- [13] S. Clatici, E. Chien, and J. Solomon. Stochastic Wasserstein Barycenters. In *ICML*, 2018. Cited on page 3.
- [14] M. Cuturi. Sinkhorn Distances: Lightspeed Computation of Optimal Transport. In *NeurIPS*, 2013. Cited on pages 2–4.
- [15] M. Cuturi and A. Doucet. Fast Computation of Wasserstein Barycenters. In *ICML*, 2014. Cited on pages 1, 3, 7, 8.
- [16] D. Davis and D. Drusvyatskiy. Stochastic Subgradient Method Converges at the Rate $\mathcal{O}(k^{-1/4})$ on Weakly Convex Functions. *arXiv:1802.02988*, 2018. Cited on pages 6, 7.
- [17] P. Dognin, I. Melnyk, Y. Mroueh, J. Ross, C. D. Santos, and T. Sercu. Wasserstein Barycenter Model Ensembling. In *ICLR*, 2019. Cited on page 1.
- [18] P. Dvurechenskii, D. Dvinskikh, A. Gasnikov, C. Uribe, and A. Nedich. Decentralize and Randomize: Faster Algorithm for Wasserstein Barycenters. In *NeurIPS*. 2018. Cited on page 3.
- [19] G. K. Dziugaite, D. M. Roy, and Z. Ghahramani. Training Generative Neural Networks via Maximum Mean Discrepancy Optimization. In *UAI*, 2015. Cited on page 5.
- [20] C. Frogner, C. Zhang, H. Mobahi, M. Araya-Polo, and T. Poggio. Learning with a Wasserstein Loss. In *NeurIPS*, 2015. Cited on page 1.
- [21] A. Genevay, L. Chizat, F. Bach, M. Cuturi, and G. Peyré. Sample Complexity of Sinkhorn Divergences. In *AISTATS*, 2019. Cited on page 3.
- [22] A. Genevay, G. Peyre, and M. Cuturi. Learning Generative Models with Sinkhorn Divergences. In *AISTATS*, 2018. Cited on pages 3–5.
- [23] A. Gramfort, G. Peyré, and M. Cuturi. Fast Optimal Transport Averaging of Neuroimaging Data. In *IPMI*, 2015. Cited on pages 1, 9.
- [24] A. Gretton, O. Bousquet, A. Smola, and B. Schölkopf. Measuring Statistical Dependence with Hilbert-Schmidt Norms. In *COLT*, 2005. Cited on pages 2, 4.
- [25] I. Gulrajani, F. Ahmed, M. Arjovsky, V. Dumoulin, and A. C. Courville. Improved Training of Wasserstein GANs. In *NeurIPS*. 2017. Cited on page 5.
- [26] H. Janati, M. Cuturi, and A. Gramfort. Wasserstein Regularization for Sparse Multi-Task Regression. In *AISTATS*, 2019. Cited on page 9.
- [27] L. V. Kantorovich. On the Translocation of Masses. *Journal of Mathematical Sciences*, 5(1):14, 1958. Cited on page 3.
- [28] C.-L. Li, W.-C. Chang, Y. Cheng, Y. Yang, and B. Póczos. MMD GAN: Towards Deeper Understanding of Moment Matching Network. In *NeurIPS*. 2017. Cited on page 5.
- [29] G. Luise, A. Rudi, M. Pontil, and C. Ciliberto. Differential Properties of Sinkhorn Approximation for Learning with Wasserstein Distance. In *NeurIPS*. 2018. Cited on page 7.
- [30] G. Luise, S. Salzo, M. Pontil, and C. Ciliberto. Sinkhorn Barycenters with Free Support via Frank-Wolfe Algorithm. In *NeurIPS*. 2019. Cited on pages 1, 3, 7, 8, 15.
- [31] R. J. McCann. A Convexity Principle for Interacting Gases. *Advances in Mathematics*, 128(1):153–179, 1997. Cited on page 2.
- [32] G. Monge. Mmoire sur la Thorie des Dblais et des Remblais. In *Histoire de lAcadmie Royale des Sciences de Paris*. Volume s1-14, pages 139–143. 1781. Cited on page 3.
- [33] K. Muandet, K. Fukumizu, B. Sriperumbudur, and B. Schölkopf. Kernel Mean Embedding of Distributions: A Review and Beyond. *Foundations and Trends in Machine Learning*, 10(1-2):1–141, 2017. Cited on page 4.
- [34] G. Peyr and M. Cuturi. Computational Optimal Transport. *Foundations and Trends in Machine Learning*, 11(5-6):355–607, 2019. Cited on page 14.
- [35] G. Peyr, M. Cuturi, and J. Solomon. Gromov-Wasserstein Averaging of Kernel and Distance Matrices. In *ICML*, 2016. Cited on pages 1, 2.
- [36] M. Sanjabi, J. Ba, M. Razaviyayn, and J. Lee. On the Convergence and Robustness of Training GANs with Regularized Optimal Transport. In *NeurIPS*, 2018. Cited on pages 6, 7, 12.
- [37] R. Sinkhorn. Diagonal Equivalence to Matrices with Prescribed Row and Column Sums. In volume 45 of number 2, pages 195–198, 1974. Cited on page 3.
- [38] S. Srivastava, V. Cevher, Q. Dinh, and D. Dunson. WASP: Scalable Bayes via Barycenters of Subset Posteriors. In *AISTATS*, 2015. Cited on page 1.

- [39] M. Staib, S. Clatici, J. M. Solomon, and S. Jegelka. Parallel Streaming Wasserstein Barycenters. In *NeurIPS*. 2017. Cited on page [3](#).
- [40] Y. Su, S. Zhao, X. Chen, I. King, and M. Lyu. Parallel Wasserstein Generative Adversarial Nets with Multiple Discriminators. In *IJCAI*, 2019. Cited on page [5](#).
- [41] C. Villani. *Optimal Transport: Old and New*, volume 338. Springer Science & Business Media, 2008. Cited on pages [2](#), [14](#).

A Proof of Propositions 4 and 6

We start by introducing some key notation. We denote by \mathcal{E} the set of discriminators f in the optimized MMD

$$SMMD^2(G_\theta, \mu) := \sup_{f \in \mathcal{E}} MMD_f^2(G_{\theta\#\rho}, \nu). \quad (17)$$

We next state the assumptions that will be used in the following.

1. \mathcal{E} is parametrized by a compact set of parameters Ψ and any $f \in \mathcal{E}$ is continuous w.r.t. those parameters.
2. Functions in \mathcal{E} are jointly continuous w.r.t. (ψ, \mathbf{x}) and are L -Lipschitz and L -Lipschitz smooth w.r.t. to the input \mathbf{x} , i.e.,

$$\|f_\psi(\mathbf{x}) - f_\psi(\mathbf{x}')\| \leq L\|\mathbf{x} - \mathbf{x}'\|, \quad (18)$$

$$\|\nabla_{\mathbf{x}} f_\psi(\mathbf{x}) - \nabla_{\mathbf{x}} f_\psi(\mathbf{x}')\| \leq L\|\mathbf{x} - \mathbf{x}'\|. \quad (19)$$

3. There exists a square integrable function $a : \mathcal{Z} \rightarrow \mathbb{R}$ and an integrable function $b : \mathcal{Z} \rightarrow \mathbb{R}$, such that generators $\theta \mapsto G_\theta(z)$ are a -Lipschitz and b -Lipschitz smooth in the following sense:

$$\|G_\theta(z) - G_{\theta'}(z)\| \leq |a(z)|\|\theta - \theta'\|, \quad (20)$$

$$\|\nabla_{\theta} G_\theta(z) - \nabla_{\theta} G_{\theta'}(z)\| \leq |b(z)|\|\theta - \theta'\|. \quad (21)$$

Moreover, for all $h \in \mathcal{E}$ and $\theta \in \Theta$ the square integral of a and integral of b are uniformly bounded by some constant C so that

$$\int |a(z)|^2 p_{h,\theta} \circ g_\theta d\eta \leq C, \quad (22)$$

$$\int |b(z)| p_{h,\theta} \circ g_\theta d\eta \leq C. \quad (23)$$

4. G_θ is L -Lipschitz and L -Lipschitz smooth in θ uniformly in z .
5. The input and output spaces are compact.
6. The kernel is L -smooth and L -Lipschitz.

Proposition 8. *Under assumptions 2, 3 and 6, we have that $\mathcal{M}(\theta) := MMD_f^2(G_{\theta\#\rho}, \mu)$ is Lipschitz and Lipschitz smooth uniformly on \mathcal{E} , i.e.,*

$$|\mathcal{M}_\theta(f) - \mathcal{M}_{\theta'}(f)| \leq L\|\theta - \theta'\| \quad (24)$$

$$\|\nabla \mathcal{M}_\theta(f) - \nabla \mathcal{M}_{\theta'}(f)\| \leq L\|\theta - \theta'\|. \quad (25)$$

Proof: Recall that under assumptions 2, 3 and 6, the dominated convergence theorem guarantees that $\mathcal{M}_\theta(f)$ is differentiable in θ , with a gradient

$$\nabla_{\theta} \mathcal{M}_\theta(f) = 2 \left(\int \nabla_1 k(f \circ G_\theta(z), f(\mathbf{x})) R_\theta(z) d\mu(\mathbf{x}) d\rho(z) \right. \quad (26)$$

$$\left. - \int \nabla_1 k(f \circ G_\theta(z), f \circ G_\theta(z)) R_\theta(z) d\mu(\mathbf{x}) d\rho(z) \right), \quad (27)$$

where $R_\theta(z) = \nabla f(G_\theta(z)) \nabla_{\theta} G_\theta(z)$. Moreover, the gradient can be upper-bounded uniformly in f since f , G_θ and k are all Lipschitz. This implies that $\theta(f)$ is Lipschitz uniformly in f . The fact that $\nabla \mathcal{M}_\theta(f)$ is uniformly Lipschitz also results the fact that gradients of f , G_θ and k are all Lipschitz.

Proof of Proposition 4. Here, we use [36] (Theorem 3.1), which guarantees that the entropy-regularized Wasserstein distance is smooth as soon as Assumptions 4 and 5 hold. This implies that the Sinkhorn divergence is also smooth and, finally, that $\theta \mapsto L(\theta)$ is smooth as a convex combination of smooth functions.

Proof of Proposition 6. We will only prove that the optimized MMD is L -weakly convex. The resulting loss L will then also be weakly convex for a suitable constant as it is simply a convex combination of weakly convex terms. For simplicity, we denote $\mathcal{SM}_\theta := \text{SMMD}^2(G_{\theta\#\rho}, \mu)$.

Using Proposition 8, we know that $\mathcal{M}(\theta) := \text{MMD}_f^2(G_{\theta\#\rho}, \mu)$ is C -smooth. It is therefore weakly convex and the following inequality holds:

$$\mathcal{M}_{\theta_t}(f) \leq t\mathcal{M}_\theta(f) + (1-t)\mathcal{M}_{\theta'}(f) + \frac{C}{2}t(1-t)\|\theta - \theta'\|^2. \quad (28)$$

Taking the supremum w.r.t. f , it follows that

$$\mathcal{SM}(\theta_t) \leq t\mathcal{SM}(\theta) + (1-t)\mathcal{SM}(\theta') + \frac{C}{2}t(1-t)\|\theta - \theta'\|^2. \quad (29)$$

This means exactly that \mathcal{SM} is weakly convex.

The fact that \mathcal{SM} is Lipschitz, is a consequence of Proposition 8. Indeed, $\mathcal{M}_\theta(f)$ is Lipschitz in θ uniformly on \mathcal{E} . Hence,

$$\mathcal{M}_\theta(f) \leq \mathcal{M}_{\theta'}(f) + C\|\theta - \theta'\|. \quad (30)$$

Taking the supremum over f , it follows directly that

$$\mathcal{SM}(\theta) \leq \mathcal{SM}(\theta') + C\|\theta - \theta'\|. \quad (31)$$

By exchanging the roles of θ and θ' , we get the other side of the inequality. $\mathcal{SM}(\theta)$ is indeed Lipschitz in θ and by the Rademacher theorem, \mathcal{SM} is even differentiable for almost all θ .

B Proof of Wasserstein barycentric properties

Here we consider the barycenter problem when the \mathcal{W}_2 distance is used:

$$\min_P L(P) := \sum_k \alpha_k \mathcal{W}_2^2(P, P_k) \quad (32)$$

We will show that the optimal P exists and can be obtained by solving the multi-marginal problem

$$\min_Q \int \sum_k \alpha_k \|\mathbf{x}_k - T(\mathbf{X})\|^2 dQ(\mathbf{X}), \quad (33)$$

where $\mathbf{X} = (\mathbf{x}_1, \dots, \mathbf{x}_P)$, $T(\mathbf{X}) = \sum_k \alpha_k \mathbf{x}_k$ and Q is a coupling between $\mathbf{x}_1, \dots, \mathbf{x}_P$ with marginals given by $(P_k)_{1 \leq k \leq P}$. A key remark is that (33) is equivalent to

$$\max_Q \int \|T(\mathbf{X})\|^2 dQ(\mathbf{X}). \quad (34)$$

This is simply a consequence of expanding the square in (33) and using the definition of $T(\mathbf{X})$. We denote by Q^* the optimal solution for (33) for which we have by definition

$$\int \|T(\mathbf{X})\|^2 dQ^*(\mathbf{X}) \geq \int \|T(\mathbf{X})\|^2 dQ(\mathbf{X}) \quad (35)$$

for all multi-marginal coupling Q of $(P_k)_{1 \leq k \leq P}$.

Consider now $P^* = T_{\#}Q^*$ where a sample \mathbf{Y} is obtained by first sampling \mathbf{X} according to Q^* and then setting $\mathbf{Y} = T(\mathbf{X})$. We obtain an upper bound on $L(P^*)$ via

$$\begin{aligned} L(P^*) &= \sum_k \alpha_k \mathcal{W}_2^2(P^*, P_k) \\ &\leq \sum_k \alpha_k \int \|T(\mathbf{X}) - \mathbf{x}_k\|^2 dQ^*(\mathbf{X}) \\ &= \int \left(\sum_k \alpha_k \|\mathbf{x}_k\|^2 - \|T(\mathbf{X})\|^2 \right) dQ^*(\mathbf{X}) \\ &= \sum_k \alpha_k \int \|\mathbf{x}_k\|^2 dP_k(\mathbf{x}_k) - \int \|\mathbf{Y}\|^2 dP^*(\mathbf{Y}). \end{aligned}$$

The second line is obtained by using the fact that $(T, Proj_k)_\# Q^*$ defines a coupling between P^* and P_k . The third and last lines are expansions recalling that the marginals of Q^* are P_k and that $P^* = T_\# Q$.

Now, let P be any probability distribution with finite second moment. It is well known that there exist optimal couplings π_k between P and each P_k , such that

$$\mathcal{W}_2^2(P, P_k) = \int \|\mathbf{Y} - \mathbf{x}_k\|^2 d\pi_k(\mathbf{Y}, \mathbf{x}_k). \quad (36)$$

Moreover, by Proposition 9, we know there exists a joint coupling π between $(\mathbf{Y}, \mathbf{x}_1, \dots, \mathbf{x}_P)$ with pairwise marginals given by π_k . Hence, $L(P)$ can be expressed as

$$L(P) = \int \sum_k \alpha_k \|\mathbf{Y} - \mathbf{x}_k\|^2 d\pi(\mathbf{Y}, \mathbf{X}) \quad (37)$$

$$= \int \left(\|\mathbf{Y}\|^2 - 2\mathbf{Y}^\top T(\mathbf{X}) + \sum_k \alpha_k \|\mathbf{x}_k\|^2 \right) d\pi(\mathbf{Y}, \mathbf{X}) \quad (38)$$

$$= \int \|\mathbf{Y}\|^2 dP(\mathbf{Y}) - 2 \int \mathbf{Y}^\top T(\mathbf{X}) \pi(\mathbf{Y}, \mathbf{X}) + \sum_k \alpha_k \int \|\mathbf{x}_k\|^2 dP_k(\mathbf{x}_k). \quad (39)$$

The first line is by definition of the coupling π , the second line is a simple expansion of the square function and last line uses that π has marginals given by P and $(P_k)_{1 \leq k \leq P}$.

Using the preceding expressions, we now compute a lower bound on the difference $L(P) - L(P^*)$ as

$$L(P) - L(P^*) \geq \int \|\mathbf{Y}\|^2 dP(\mathbf{Y}) - 2 \int \mathbf{Y}^\top T(\mathbf{X}) \pi(\mathbf{Y}, \mathbf{X}) + \int \|\mathbf{Y}\|^2 dP^*(\mathbf{Y}). \quad (40)$$

Consider now Q_0 be the distribution over \mathbf{X} obtained by marginalizing π over \mathbf{Y} . Then π is a coupling between P and Q_0 . Moreover, by definition of Q^* we have that

$$\int \|\mathbf{Y}\|^2 dP^*(\mathbf{Y}) = \int \|T(\mathbf{X})\|^2 dQ^*(\mathbf{X}) \geq \int \|T(\mathbf{X})\|^2 dQ_0(\mathbf{X}). \quad (41)$$

This directly implies that

$$L(P) - L(P^*) \geq \int \|\mathbf{Y}\|^2 dP(\mathbf{Y}) - 2 \int \mathbf{Y}^\top T(\mathbf{X}) \pi(\mathbf{Y}, \mathbf{X}) + \int \|T(\mathbf{X})\|^2 dQ_0(\mathbf{X}) \quad (42)$$

$$= \int \|\mathbf{Y} - T(\mathbf{X})\|^2 \pi(\mathbf{Y}, \mathbf{X}) \geq 0. \quad (43)$$

Proposition 9. [34, 41] *Given pairwise couplings π_k between variables $(\mathbf{Y}, \mathbf{x}_i)$ there exists a joint coupling π between $(\mathbf{Y}, \mathbf{x}_1, \dots, \mathbf{x}_P)$ that admits π_k as marginals.*

C Proof of MMD properties

Here, we consider the MMD with a fixed kernel k . Denote by $\eta(P)$ the kernel mean embedding of the distribution P , ie.: $\eta(P) = \int k(\mathbf{x}, \cdot) dP(\mathbf{x})$. We want to show that $P^* = \sum_k \alpha_k P_k$ is the minimizer of

$$\min_P \sum_k \alpha_k \|\eta(P) - \eta(P_k)\|_{\mathcal{H}}^2. \quad (44)$$

This is equivalent to finding an optimal function Φ in \mathcal{H} that minimizes

$$\min_{\Phi} \sum_k \alpha_k \|\Phi - \eta(P_k)\|_{\mathcal{H}}^2. \quad (45)$$

under the additional constraint that Φ is a mean embedding of some probability distribution P . We will show that the unconstrained problem in (45) admits $\eta(P^*)$ as an optimal solution. Equation

(45) is a strongly convex quadratic function of Φ . Therefore it admits a unique global minimum, which is given by the first-order optimality condition

$$\phi^* = \sum_k \alpha_k \eta(P_k). \quad (46)$$

Now we use the fact that the kernel mean embedding is a linear operator on measures, which implies directly that $\sum_k \alpha_k \eta(P_k) = \eta(\sum_k \alpha_k P_k) = \eta(P^*)$. We have shown that Φ^* , the unconstrained solution of (45), is a mean embedding for P^* . This directly implies that P^* is an optimal solution to (44). Uniqueness is obtained whenever the mean embedding is injective, i.e., the kernel k is characteristic.

D Algorithm

Algorithm 2 Algorithm for computing barycenters of arbitrary measures

Require: Network G_θ , measures $\{\mu_p\}_{p=1}^P$, weights $\{\beta_p\}_{p=1}^P$, base measure ρ , distances $\{D_p\}_{p=1}^P$, learning rate γ

for epoch in epochs **do**

for $p = 1, \dots, P$ **do**

 Sample minibatches $\{x_j^{(p)} \sim \mu_p\}_{j=1}^J$

 Sample $z_j \sim \rho, j = 1, \dots, J$

 Compute

$$g_p(\theta) = \nabla_\theta D_p \left(\sum_{j=1}^J \delta_{x_j^{(p)}}, \sum_{j=1}^J \delta_{G_\theta(z_j)} \right)$$

end for

 Update $\theta = \theta - \gamma \sum_{p=1}^P \beta_p g_p(\theta)$

end for

E Experimental Details

E.1 Nested Ellipses

E.1.1 Setup

We compute the Sinkhorn divergence using Geomloss. For both parametrizations, we train using the Sinkhorn divergence with entropic coefficient $\epsilon = 0.1$ and a batch size of 150. **MLP parametrization** We use a MLP with 4-hidden layers (50, 200, 1000, 200 neurons), ReLU activations, a latent dimension of 10. **Ellipse parametrization** We initialize the centers and axis of the nested ellipses from standard Gaussians.

E.1.2 Discussion

We note that if given a substantially higher time budget, the algorithm of Luise et al. [30] would converge to a significantly better solution, as per its convergence guarantees. However, because of computational time constraints, we fixed the maximum number of support points to be added to $N = 1500$, which resulted in the provided figure. By contrast, our approach leverages global basis functions, which in turn put mass on a large support directly, without having to optimize locations individually.

E.2 Gaussians

E.2.1 Setup

We plot mean and the 5%–95% quantiles (across 5 random seeds). We compute the Sinkhorn divergence using Geomloss. The entropic coefficient is set to $\epsilon = 0.01$ (so that the Sinkhorn divergence

approximates the Wasserstein well), average over 5 seeds, and use an exponential scheduler with decay parameter $\lambda = 0.985$ (the learning rate decreases every epoch). **Sinkhorn: MLP parametrization** We use a MLP with 4-hidden layers (50, 200, 1000, 200 neurons), ReLU activations, a latent dimension of 2, and the batch size to 150. We set the learning rate to 8×10^{-4} . **Sinkhorn: Gaussian parametrization** We parametrize the mean and the variance of an isotropic 2D Gaussian. We set the learning rate to 0.4 and the batch size to 150. **MMD: MLP parametrization** We use a MLP with 4-hidden layers (50, 200, 1000, 200 neurons), ReLU activations, a latent dimension of 8. We set the batch size to 400 and the decay parameter of the scheduler to 0.99.

E.2.2 Discussion

We set the learning rate of the MLP and the Gaussians parametrization to the maximum value at which optimization is stable. In turn, we could set the latter’s learning rate to a significantly larger value than the former’s.

E.3 Natural Images

On natural image datasets, we use DCGAN-like architectures for both the generator and critics (we use a different critic for each measure). For SMMD, we use the formulation of Binkowski et al. [7], in particular a mixture of rational quadratic kernel, convolutional critics, along with gradient penalty. For the CelebA experiment, we also use and spectral normalization for regularization. However, we set the critics’ output dimensions to 1 instead of 16, which leads to similar performance. We perform five critic iterations per generator iteration and train using the ADAM optimizer with $\beta_1 = 0.5$, $\beta_2 = 0.99$ and a learning rate of 2×10^{-4} . In CelebA experiments, we include an exponentially decreasing scheduling ($\gamma = 0.99$).